

# Succinct Papers

## A New Class of Medium-Size High-Efficiency Reflector Antennas

HERMANN W. EHRENSPECK

**Abstract**—The new class of reflector antennas that is described in this communication yields a higher directive gain than obtained with conventional reflector antennas of the same area. An antenna of this new design consists of a reflecting surface, a peripheral rim, and a feed system in the reflector center. It is analyzed as a combination of two radiating sources whose radiation maxima and mutual phase relations can be simply adjusted for highest directive gain in the axis normal to the reflector. The marked directive gain increase is explained on the basis that there is a virtual extension of the radiating aperture beyond the physical dimensions of the reflector. The two antenna models that are described develop directive gains of almost 3 dB above those of conventional reflector antennas of equal size and comparable pattern characteristics. Optimized for a given frequency, the new design covers a pattern bandwidth of approximately 4:1.

### I. DESCRIPTION OF ANTENNA

Experimental research was carried out with small- and medium-size center-fed reflector antennas having rims of adjustable width [1]. Fig. 1 outlines two views [(a) front, (b) cross section] of a typical circular planar reflector antenna. The diameter of the reflecting surface is denoted  $D_A$ . Feed  $F$  is located in the center of the reflector at a distance between  $d_F \approx \lambda/4$  and  $d_F \approx \lambda/2$  from  $A$ . The feed must be capable of properly illuminating the entire reflector area. Reflector areas of approximately  $2\lambda^2$  can be illuminated by a single dipole. Larger reflectors require a feed whose effective radiating aperture is larger than that of a dipole—for example, one short-backfire (SBF) feed [2], [3] or an array of them. In this model (Fig. 1), a linear dipole provides linear polarization. Crossed dipoles or any other radiator that provides the desired polarization may also be used. With a pair of crossed dipoles as the feed system, measurements indicated attenuation of approximately 30 dB between the horizontally and vertically polarized field components.

As seen in Fig. 1(b), the rim  $B$  (width =  $W_B$ ) of the experimental antenna can be moved to the right any distance  $d_B$  until it reaches its outer position (dashed lines), when  $d_B = W_B$ . The plane of the rim edge (two small circles marked  $E$ ), which also constitutes the aperture plane of the antenna, is denoted by the dotted line  $P$  extending parallel to and spaced a distance  $d_B$  in front of  $A$ .

### II. DEVELOPMENT OF OPTIMAL ANTENNA DIMENSIONS

A first series of directive gain measurements as a function of frequency in the range 1 to 4 GHz was performed on an antenna model similar to that sketched in Fig. 1. At the higher frequencies the reflector of this model was larger than  $2\lambda^2$ . Instead of the single-dipole feed, therefore, an SBF feed had to be used, that is, a dipole feed with a reflector disk in front of it. The antenna was optimized by varying the frequency and rim width  $d_B$  to find its highest directive gain. It reached 18.1 dB at  $f_m = 3.4$  GHz, with the reflector diameter  $D_A = 2.35\lambda$  and the rim width adjusted to  $d_B = 0.57\lambda$ .

With these optimum dimensions kept constant, patterns and directive gain were measured over the entire 1- to 4-GHz frequency range. Fig. 2 shows the resulting directive gain curve as a function of frequency. It also contains the directive gain curves calculated according to the well-known area-directivity equation  $G = [(4\pi A)/\lambda^2] \cdot e$ , with  $A$  as the reflector area and  $e$  denoting the ap-

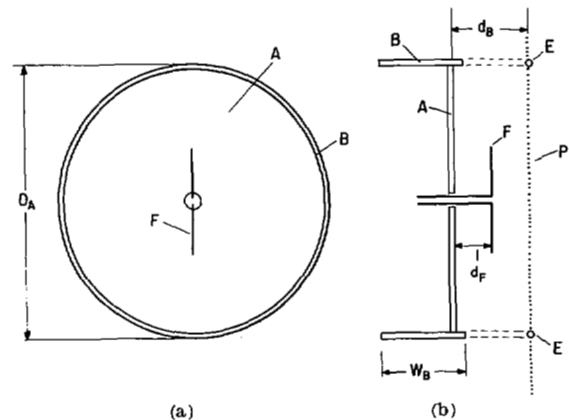


Fig. 1. Sketch of antenna. (a) Front view. (b) Cross section.

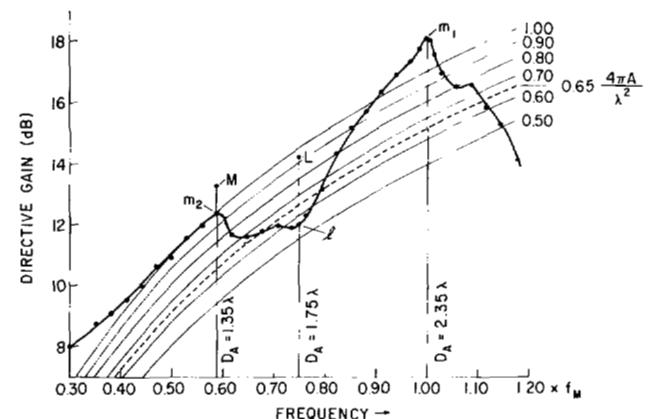


Fig. 2. Directive gain versus frequency curve.

ture illumination efficiency. Although this equation is strictly valid only for reflector areas of many square wavelengths, it can be used for obtaining the approximate directive gains of reflector antennas having smaller reflector areas.

The directive gain curves (solid lines) are shown for  $e = 0.5$  to  $e = 1.0$  in steps of 0.1. They relate the measured directive gain values to the area of the reflector and the wavelength such that the aperture illumination efficiency can be directly determined. The directive gain curve for  $e = 0.65$  (dashed line), which is normally used for approximate calculations of the gain of circular-shaped reflector antennas [4], is also shown. This curve allows an immediate directive gain comparison of the new antenna type with conventional reflector antennas having the same area and approximately the same sidelobe level.

Although the measured directive gain is continuously decreasing with frequency from its maximum  $m_1 = 18.1$  dB at  $d_A = 2.35\lambda$  and  $d_B = 0.57\lambda$ , it passes through a local minimum  $\ell$  at  $d_A = 1.75\lambda$  with the lowest aperture illumination efficiency  $e \approx 0.55$ , and reaches a second maximum  $m_2 = 12.4$  dB, with  $e \approx 1.0$  at  $d_A = 1.35\lambda$  and  $d_B = 0.34\lambda$ .

In a second series of measurements, the influence of the rim width  $d_B$  on the directive gain of the antenna was studied for several selected frequencies corresponding to reflector diameters smaller than  $2.35\lambda$ . It was found that different adjustments of the rim width produced somewhat higher directive gains for the smaller reflectors. The largest increase occurred at  $d_A = 1.75\lambda$ ; but the general characteristics of the directive gain curve (Fig. 2) were unchanged with maxima still at reflector diameters of  $1.35\lambda$  and  $2.35\lambda$ . In this set of measurements, one adjustment of the reflector rim width was

also found that produced a much smoother directive gain curve than that shown in Fig. 2. This special antenna configuration also develops a very high efficiency, and its directive gain is approximately proportional to the reflector area.

The influence of the rim width adjustment on the directive gain of the antenna in Fig. 1, can be most clearly demonstrated in those antennas whose dimensions yield the smallest directive gain because of their lowest aperture illumination efficiency.

As seen in Fig. 2, the aperture illumination efficiency is lowest—55 percent—at the frequency at which the reflector diameter is  $1.75\lambda$ . The increase in directive gain measured as a function of rim width from  $d_B = 0$  (without a rim) to  $d_B = 1.5\lambda$  (widest rim) is plotted in Fig. 3. It is noted that at  $d_B = 0.6\lambda$  the directive gain first shows an increase of 5.2 dB over the value for the rimless antenna and then, with increasing  $d_B$ , decreases to a minimum lower than that for the rimless antenna. Since the reflector diameter is far from its optimum size and its far-field contribution therefore small, it can be assumed that the behavior of the directive gain curve in Fig. 3 is caused mainly by phase changes between the far-field contributions of the edge and feed radiators. It can also be assumed that the low directive gain of the rimless antenna ( $d_B = 0$ ) indicates a phase difference of approximately  $180^\circ$  between the two radiators.

### III. TWO-RADIATOR ANALYSIS AND OPTIMIZATION OF THE ANTENNA

The diameter of the reflector and the width of the rim have proved to be the decisive parameters in optimizing the described antenna for maximum directive gain. The results suggested analyzing the antenna as a combination of two radiators—the feed in the center of the reflecting surface  $A$  and edge  $E$  of the rim in front of  $A$ . When the feed is energized, the rim is excited by radiation coupling, and its edge  $E$  acts as a secondary radiator. Proper choice of the rim dimensions allows this secondary radiator to be optimized in amplitude and phase with respect to the primary feed radiator. Since both the 'feed' radiator and the 'edge' radiator are arranged in front of the common reflector  $A$ , the directive gain accruing from their combination reaches a maximum in the plane of the axis normal to the reflecting surface. The radiation patterns of the combination can be determined by superposing the individual patterns from both sources. Highest directivity is obtained when the amplitude-optimized far-field contributions of both radiators are in phase, and lowest when they are in antiphase.

Thus the antenna in Fig. 1 can be adjusted to yield its highest directive gain for a given frequency by satisfying the following three conditions.

- 1) The diameter of the edge radiator  $E$  is such that

$$d_{A,\text{opt}} \cong (n + 0.35)\lambda, \quad n = 1, 2, 3, \dots$$

- 2) The width  $d_B$  of the rim is adjusted so that the far fields of the feed and edge radiators coincide in phase in the direction normal to the plane of reflector  $A$ .

- 3) The radiation coupling between feed  $F$  and edge radiator  $E$  is strong enough to contribute appreciably to the far field of the two-source combination.

If feed radiators of types other than dipoles are used—for example, a waveguide or a spiral—the radiation coupling [condition 3)] and the current distribution on the rim edge may be different from those of the dipole, and the antenna will therefore be optimized for rim diameters somewhat different from those given in condition 1).

### IV. TWO-RADIATOR ANALYSIS COMPARED WITH OPEN-CAVITY RADIATOR ANALYSIS

In an earlier stage of this investigation, an attempt was made to analyze the antenna in Fig. 1 as an open-cavity radiator by a method similar to that used by Hong *et al.* [5]. The large discrepancies between our results and theirs, however, indicate that their theory does not seem to apply to the antennas described here, most likely for the following reasons.

First, for a favorable excitation of propagating cavity modes, Hong *et al.* assumed much higher cavity walls than we did (see Section III and Fig. 3). Second, they decided to neglect the diffraction and coupling effects at the radiating cavity end (rim edge). According to our results, these effects have a most decisive influence on the directive gain. Third, in contrast to the procedure followed in our work, they apparently did not investigate the in-

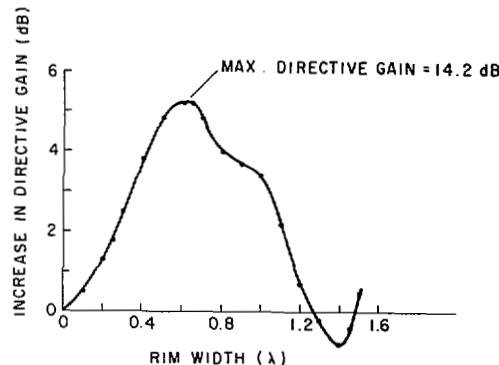


Fig. 3. Effect of rim width on directive gain.

fluence of the height of the cavity wall on pattern performance nor did they direct their analysis toward a directive-gain optimization of their antennas.

In another study Hsieh *et al.* [6] applied a 'numerical-physical optics' method to determine the radiation characteristics of a SBF antenna of  $2\lambda$  diameter, similar in structure to that in Fig. 1, except that it had a secondary reflector as necessitated by the primary reflector size (see Section II). In their analysis they, too, considered the effect of the rim edge. As a first step they calculated the radiation patterns of a rimless antenna. As a second step they added the rim as a cavity wall and introduced a correction term based on the field diffracted by the rim edge. From their results, they reported [6] that the rim-diffracted fields do not cause any significant changes in the antenna patterns or its directive gain. Our results, on the contrary, indicate a very significant increase in directive gain when the rim edge is added and its dimensions optimized. Optimization was not attempted in the work reported in [6].

To sum up, our experimental results cannot be satisfactorily explained by analyzing our antenna as an open-cavity radiator. A search of the literature has turned up no theory that gives full consideration to the effect of the rim edge radiation and its phase relations with the antenna feed or explains the large directive gain increase obtained by using a rim of optimized dimensions.

### V. PATTERNS OF OPTIMIZED ANTENNA BEFORE AND AFTER DIRECTIVE GAIN ADJUSTMENT

The directive gain increase obtained by the optimization adjustments of the described reflector antenna cannot be accurately predicted at the present time because of complicated interactions between all parameters. It can, however, be clearly demonstrated in comparisons of the  $E$ - and  $H$ -plane patterns and the measured directive gains before and after the optimizing procedure is performed.

Fig. 4(a) shows typical  $E$ - and  $H$ -plane radiation patterns of an antenna like the one sketched in Fig. 1, optimized to a reflector diameter of  $1.35\lambda$ . Comparing the half-power beamwidths of the antenna that has an optimized rim with that of the rimless antenna, we find that the optimized rim caused a narrowing from  $54^\circ$  to  $40^\circ$  in the  $E$ -plane and from  $80^\circ$  to  $48^\circ$  in the  $H$ -plane, and increased the directive gain by approximately 3.5 dB to a maximum of 13.3 dB ( $M$  in Fig. 2). Even greater increases in directive gain were measured with the  $1.75\lambda$  antenna whose rim-optimization curve is given in Fig. 3. The radiation patterns of this antenna [Fig. 4(b)] show that rim optimization narrowed the half-power beamwidth from  $65^\circ$  to  $42^\circ$  in the  $E$ -plane and from  $104^\circ$  to  $32^\circ$  in the  $H$ -plane. The directive gain maximum ( $L$  in Fig. 2) measured 14.2 dB.

The marked improvement in performance afforded by the new class of antennas is obvious when the directive gain and efficiency are compared with the directive gain and efficiency of other types of reflector antennas. If we assume the theoretically highest aperture illumination efficiency  $e = 1.00$ , an antenna built according to Fig. 1, with a diameter of  $1.35\lambda$  (hence a reflector area of  $1.43\lambda^2$ ), should have a calculated directive gain of 18.0 (12.5 dB). The measured value, however, is 21.4 (13.3 dB). The increase in directive gain cannot be explained on the basis of an increase in aperture illumination efficiency since  $e = 1.00$  implies 100 percent illumination with a constant field amplitude over the total physical reflector area. Furthermore, any such increase would have had to be obtained at

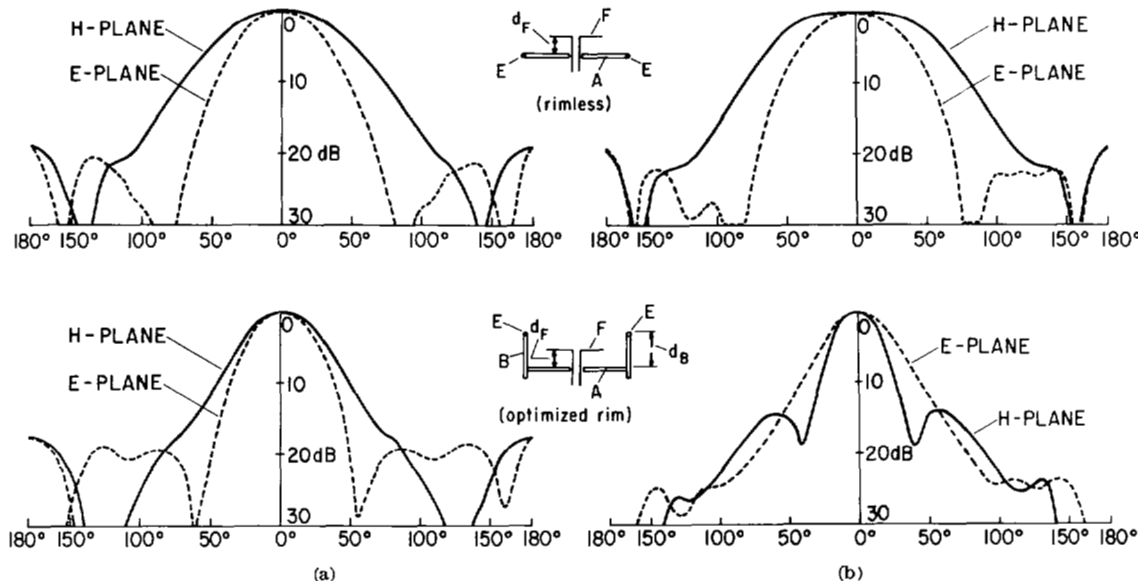


Fig. 4. *E*- and *H*-plane radiation patterns before and after optimum directive gain adjustment [(a)  $D_A = 1.35\lambda$ ; (b)  $D_A = 1.75\lambda$ ].

the expense of a relatively high sidelobe level, whereas our antenna models have, on the contrary, always yielded favorably low sidelobes. The increase in directive gain was therefore assumed to be the result of a virtual extension of the physical radiating aperture of the optimized antenna to a larger effective aperture, attributable to the radiation field of the optimized rim. This assumption seems to be verified by the following measurements of aperture fields of the antenna model (Fig. 1) with  $D_A = 1.35\lambda$ .

To explore the aperture fields, a small dipole probe was moved in a plane parallel to  $A$  and spaced a distance of  $0.25\lambda$  from the rim edge  $E$ . The maximum field amplitude for both the *E*- and *H*-plane measurements was adjusted to the same value, with the probe located in the normal axis of the antenna.

The results are presented in Fig. 5, showing Fig. 5(a) the configuration and Fig. 5(b) the field distribution across the aperture measured in the *E*- and *H*-planes of the feed radiator. Although the two curves would be better presented in a three-dimensional coordinate system because they are measured in two orthogonal planes, both are shown together in the  $xy$  coordinate system for simplicity. The plane of the probe movement (dashed-dotted line) is taken as the  $x$  axis; the normal axis of the reflector is the  $y$  axis.

It is noted that the radiating aperture of the antenna extends far outside the physical dimensions of the structure and the power has decreased by 20 dB from that in the antenna axis at distances of approximately  $0.4\lambda$  from the edge of the rim at points  $h$  on the  $x$  axis in the *E*-plane, and approximately  $0.9\lambda$  at points  $v$  in the *H*-plane. This information is not sufficient for calculating the directive gain increase because the phase distribution across the entire aperture would also need to be known and taken into account. The distribution curves do, however, indicate that the radiating aperture of the antenna has been significantly extended by the optimizing procedure and that a marked increase in directive gain can thus be expected.

Similar results were measured with a reflector diameter of  $2.35\lambda$  (with an SBF feed). Calculated according to its area  $A = 4.32\lambda^2$ , its directive gain is 54.2 (17.3 dB) for  $e = 1.0$ , and 35 (15.4 dB) for  $e = 0.65$ , compared with a measured value of 65 (18.1 dB). The half-power beamwidths are  $24.5^\circ$  and  $23.5^\circ$  in the *E*- and *H*-plane patterns, respectively, and the directive gain is 2.9 dB above that calculated for  $e = 0.65$  [4].

## VI. PATTERN BANDWIDTH OF ANTENNA

The frequency-dependent directive-gain adjustment could be expected to limit the antenna to narrow-bandwidth applications. The directive gain curve of Fig. 2 and the corresponding *E*- and *H*-plane patterns show, however, that the new type of antenna delivers superior performance over a wide frequency range. Normalized with reference to  $f_M$  for which the  $2.35\lambda$  antenna is optimized,

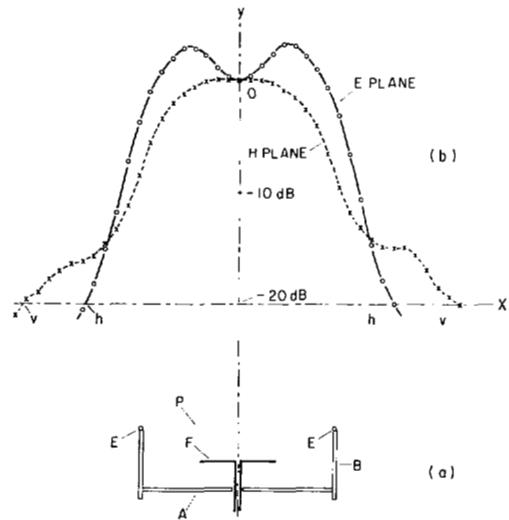


Fig. 5. Amplitude distribution in aperture of antenna.

it covers a frequency range of approximately 4:1. All sidelobes in both planes are mostly below  $-20$  dB and reach levels up to  $-10$  dB only at the highest frequencies. (Because of lack of space, radiation patterns are not included with this communication.)

A matching network for the entire 4:1 frequency range has not yet been developed. The described antenna models have, however, been impedance-matched to  $50\Omega$  for a voltage standing-wave ratio lower than 1.8:1 over a 2:1 frequency range. Best results were obtained with a broad-band dipole feed with a bifilar-coil balun in its center.

## VII. CONCLUSIONS

The reported results indicate that the described new class of reflector antennas develops significantly higher directive gains than conventional reflector antennas of the same area. The marked increase appears to be due to a virtual extension of the effective radiating aperture beyond the physical dimensions of the reflectors. The described antenna models are for areas smaller than approximately  $6\lambda^2$ , energized by a single-element feed radiator. Larger reflectors must be illuminated by an array of separately energized elements in the center area of the reflector. The multifeed arrangement often leads to reflector shapes that only approximate a circle (square or polygon with rounded edges). Two antennas of this type, one with 4 and one with 16 fed elements, developed their

highest directive gains of 20 and 25 dB, respectively, when their peripheral rim length was the same as that of a circular reflector of  $3.35\lambda$  for the first [7] and  $6.35\lambda$  for the second [8].

#### ACKNOWLEDGMENT

The author wishes to thank Dr. R. B. Mack and Dr. R. J. Mailloux for many helpful discussions and J. A. Strom for his assistance in the measurements.

#### REFERENCES

- [1] H. W. Ehrenspeck, *Optimized Reflector Antenna*, Patents applied for, Feb. 1972.
- [2] ———, "The short-backfire antenna," *Proc. IEEE*, vol. 53, pp. 1138-1140, 1965; U. S. Patents 3 438 043 and 3 508 278.
- [3] H. W. Ehrenspeck and J. A. Strom, "The short-backfire antenna as an element for high-gain arrays," USAF Cambridge Res. Labs., Bedford, Mass., Rep. AFCRL-71-0234, 1971.
- [4] H. Jasik, *Antenna Engineering Handbook*. New York: McGraw-Hill, 1961, ch. 12, p. 13.
- [5] M. H. Hong, D. P. Nyquist, and K. M. Chen, "Radiation fields of open-cavity radiators and a backfire antenna," *IEEE Trans. Antennas Propagat.*, vol. AP-18, pp. 813-815, Nov. 1970.
- [6] T. Z. Hsien, D. P. Nyquist, and K. M. Chen, "The short-backfire antenna: A numerical-physical optics study of its characteristics," USAF Contract F19628-70-C-0072, 1970.
- [7] H. W. Ehrenspeck and J. A. Strom, "The four-element SBF array: variation of parameters for optimization of performance," USAF Cambridge Res. Labs., Bedford, Mass., Rep. AFCRL-71-0569, 1971.
- [8] ———, "A sixteen-element SBF array," USAF Cambridge Res. Labs., Bedford, Mass., Rep. AFCRL-72-0500, 1972.

## 50 Ω Log-Periodic Monopole Array with Modulated-Impedance Microstrip Feeder

PHILIP B. GREEN AND PAUL E. MAYES

**Abstract**—It is demonstrated theoretically and experimentally that a log-periodic monopole array with a meander-line feeder may be expected to exhibit high values of voltage standing-wave ratio. Improved match can be obtained by allowing the impedance of the feeder to go to a higher value near each monopole. A good match to  $50 \Omega$  is achieved in this way.

#### I. INTRODUCTION

In some applications it is desired to have a vertically polarized frequency independent antenna operating over a ground plane. Since the earliest frequency-independent antennas did not have the proper symmetry, considerable effort was expended before a successful monopole array was obtained. Several types of log-periodic (LP) monopole arrays have been proposed. However, most of these tend to be design critical, that is, they perform satisfactorily over a narrow range of design parameters and have a tendency to be sensitive to construction tolerances.

The LP dipole array [3] performs well over a wide range of design parameters. An LP array of monopoles would be expected to have similar properties provided it could be fed in the same manner. However, it is not possible in an LP monopole array to achieve the exact analog of the transposed feeder used in the LP dipole array. The effect of the transposed feeder can be approximated by using excess lengths of feed line. Ordinarily this leads to problems due to reflections occurring between the feed point and the active region. A technique suggested by Ingerson and Mayes [2] for minimizing the reflections is applied here to the realization of a meandering microstrip feed for an LP monopole array with  $50\Omega$  input impedance. The impedance of the microstrip feeder is increased in the vicinity of each monopole to approximately match each short monopole-loaded sec-

Manuscript received April 11, 1973; revised October 19, 1973. This work was supported in part by the Andrew Corporation, Orland Park, Ill., through an Industrial Research Assistantship.

P. B. Green was with the Electromagnetics Laboratory, Department of Electrical Engineering, University of Illinois, Urbana. He is now with Central Antenna Laboratory, Texas Instruments Incorporated, Dallas, Tex.

P. E. Mayes is with the Electromagnetics Laboratory, Department of Electrical Engineering, University of Illinois, Urbana, Ill. 61801.

tion to  $50 \Omega$ . The antenna structure with meandering modulated-impedance microstrip feeder is shown in Fig. 1.

The excess lengths of feed line introduced to achieve proper phasing in the active region can result in a nonpropagating portion of the array transmission region. Cells of the LP structure in the non-propagating region can be considered to be operating in a structural stop band. The characteristics of each cell can be determined approximately by finding the dispersion characteristics of a single symmetric two-port network composed of a section of transmission line and a shunt admittance representing the monopole loading [2], [4]. The propagation characteristics of the single cell can also be interpreted for a series of cascaded two-port cells (the analytical model of the array). In doing this, the possibility of attenuating cells between the feed point and the active region of the array becomes evident.

For a series of cascaded LP two-port networks operating in a passband, each cell is very nearly terminated in its image impedance, which is real. Reflections at the cell junctions are minimal. However, the image impedance of a cell in a stopband is complex. Thus if one of the cascaded LP cells is attenuating, a poor match to adjacent cells and energy reflection result. Since the first structural stopband generally occurs in the transmission region where currents are relatively high, the reflections may be significant, causing high input VSWR.

The technique for minimizing the effect of the first structural stop band utilizes a symmetrical loaded cell with line sections of differing characteristic impedances (e.g., cell  $n$  in Fig. 2). The characteristic equation for the modulated impedance cell is [2], [4]

$$\cosh \gamma d = \cosh \gamma_1 d_1 \cosh \gamma_2 d_2 + \frac{1}{2} \left( \frac{Z_2}{Z_{11}} + \frac{Z_{11}}{Z_2} \right) \sinh \gamma_1 d_1 \sinh \gamma_2 d_2 \quad (1)$$

where  $\gamma$ ,  $\gamma_1$ , and  $\gamma_2$  are propagation constants for the cell, subcell, and line 2, respectively, and  $Z_{11}$  is the image impedance of the subcell

$$Z_{11} = Z_1 \left[ \frac{\sin \beta_{11} d_1 + j \frac{1}{2} Y_a Z_1 (1 - \cos \beta_{11} d_1)}{\sin \beta_{11} d_1 - j \frac{1}{2} Y_a Z_1 (1 + \cos \beta_{11} d_1)} \right]^{1/2}. \quad (2)$$

At the frequency at which maximum attenuation occurs in the first stopband (for the unmodulated line where  $Z_1 = Z_2$ ), the subcell parameters should be chosen so that the subcell image impedance is approximately equal to  $Z_2$ . The characteristic equation is simplified as follows (assuming lossless lines)

$$\cosh \gamma d = \cosh (\gamma_1 d_1 + j \beta_{12} d_2). \quad (3)$$

Thus if the length  $d$  is such that the first stopband is eliminated for the subcell, the structural stopband for the modulated cell will be minimized [2], [4].

#### II. THEORETICAL ANALYSIS

The network approach to analyzing an LP structure, introduced by Carrel [1], can be applied to the LP monopole array [4]. In this approach, the  $N$ -element array is modeled as the parallel combination of two circuits—an  $N$ -port network representing the antenna elements and an  $N$ -port feed circuit consisting of  $N-1$  cascaded feed cells. The monopole base currents can be calculated providing the element impedance and the feed-line admittance matrices have been computed.

$$\bar{I}_A = [\bar{U} + \bar{Z}_A \bar{Y}_F]^{-1} \bar{I} \quad (4)$$

where  $\bar{I}_A$  is a column vector of antenna base currents,  $\bar{U}$  is an identity matrix,  $\bar{Z}_A$  is the matrix of self- and mutual-antenna impedances,  $\bar{Y}_F$  is the admittance matrix of the feeder network, and  $\bar{I}$  is the column vector of driving currents.

Only the  $N$ th element of  $\bar{I}$  is nonzero (arbitrarily, one ampere). Solving (4) and assuming a sinusoidal current distribution allows the computation of the far-field radiation characteristics of the array.

The element impedance matrix  $\bar{Z}_A$  is determined using the method of induced electromotive force [5]. Two approximations are made—the induced currents in the intervening elements are neglected and sinusoidal current distributions are assumed. Both assumptions are of questionable validity for the closely spaced elements of the array and introduce a degree of discrepancy between experimental and theoretical results, but are nevertheless useful since they yield a